



PCCP

Size-dependent Photoinduced Transparency in Colloidal CdTe Quantum Dots in the Strong Confinement Regime: An inverse linear relationship

Journal:	<i>Physical Chemistry Chemical Physics</i>
Manuscript ID	CP-ART-10-2022-005006.R1
Article Type:	Paper
Date Submitted by the Author:	29-Nov-2022
Complete List of Authors:	dos Santos, Carlos Henrique; UNIFAL-MG; USP IfSC Ferreira, Diego; UNIFAL-MG Zucolotto Cocca, Leandro Henrique; Universidade de Sao Paulo Instituto de Fisica de Sao Carlos Mourão, Rafael S.; Universidade Federal de São João del-Rei Schiavon, Marco ; Universidade Federal de Sao Joao del-Rei, Ciências Naturais (DCNat) Mendonca, Cleber R.; Univ Sao Paulo, FCM De Boni, Leonardo; Instituto de Física de São Carlos - Universidade de São Paulo, Física e Ciência dos Materiais Vivas, Marcelo; Universidade Federal de Alfenas

SCHOLARONE™
Manuscripts

Size-dependent Photoinduced Transparency in Colloidal CdTe Quantum Dots in the Strong Confinement Regime: An inverse linear relationship

Carlos H. D. dos Santos,^{1,2} Diego L. Ferreira,¹ Leandro H. Zucolotto Cocca,² Rafael S. Mourão,³ Marco A. Schiavon,³ Cleber R. Mendonça², Leonardo de Boni^{2,*}, and Marcelo G. Vivas^{1,*}

¹Laboratório de Espectroscopia Óptica e Fotônica, Universidade Federal de Alfenas, Poços de Caldas, MG, Brazil

²Instituto de Física de São Carlos, Universidade de São Paulo, Caixa Postal 369, 13560-970 São Carlos, SP, Brazil

³Grupo de Pesquisa em Química de Materiais, Universidade Federal de São João del-Rei, São João del-Rei. MG, Brazil

Correspondent author: *mavivas82@gmail.com and deboni@ifsc.usp.br

ABSTRACT

Nanomaterials have been investigated as saturable absorbers for ultrafast lasers because of their large photoinduced transparency related to ground-state bleaching. However, the quantum dot size effect on the photoinduced transparency in the strong confinement regime has not been explored due to the challenge of accurately measuring the ground state and the excited-state absorption cross-sections. At the same time, these optical properties are essential to calculate several chemical and physical quantities at the nanoscale. In this context, we have employed the photoluminescence saturation method to determine the ground-state absorption cross-section and the femtosecond open-aperture Z-scan technique to investigate the size-dependent ground-state bleaching of glutathione-capped CdTe QDs synthesized in an aqueous medium. The results were modeled using rate equations within the three-energy levels approach. Our results pointed out that the photoinduced transparency rate at the $1S_{3/2}(h) \rightarrow 1S(e)$ transition peak presents an inverse linear relationship with the QD diameter (from 2.2 nm up to 3 nm). Otherwise, the larger QDs have a higher ground-state cross-section, which is directly proportional to the ground-state bleaching. To explain this apparent contradiction, we calculate the effective absorption coefficient $\alpha_{\text{eff}} = \sigma/V$ (σ is the absorption cross section and V is the QD volume) for the QDs and observed that the smaller QDs have a higher absorption from the ground to the first excited state, corroborating our results. Finally, our results showed that the saturable absorption effect in CdTe-QDs is slightly higher than that obtained for graphene and other 2D materials and smaller than the black phosphorus in the visible region.

I – INTRODUCTION

Nanomaterials have emerged in the last few decades as a multidisciplinary and disruptive research field, both from the point of view of basic science and technological applications. Within the plethora of extensively investigated nanoscale materials, semiconductor nanocrystals with radii smaller than the bulk exciton Bohr radius (called quantum dots - QDs) exhibit enhanced size-dependent optical properties that deviate substantially from those of bulk crystals, as a consequence of the reduced finite spatial dimensions and the characteristic excitonic confinement effect. For example, QDs present high linear, excited state and two-photon absorption, large nonlinear refractive index, bright fluorescence quantum yield, and large exciton binding energy, to cite a few.¹⁻¹⁴ Due to these remarkable features, QDs have been used in many applications spanning from biology to quantum information.¹⁵⁻²²

The interaction between the intense electromagnetic field delivered from the ultrashort laser pulses with matter is an interesting research topic because it allows us to modulate the optical properties of materials through laser intensity. For example, the material absorption coefficient (α) can decrease or increase depending on the excited-state dynamics at the resonant regime. When the excited-state absorption is higher than the ground-state one, α increases with the laser irradiance, which is called reverse saturable absorption (RSA). Such an effect is closely related to developing all-optical technologies such as optical power limiting, optical storage, and so on. On the other hand, when α decreases as the laser irradiance increases, we have the saturable absorption (SA), which is induced by electron population bleaching from the ground- to the excited state.^{23, 24} Such a process strongly depends on the laser pulse temporal width and excited-state lifetime; therefore, it is a purely excited-state effect. SA is commonly used in the development of lasers to decrease the laser pulse temporal width and as a nonlinear filter to clean up pulse shapes.^{23, 25, 26} Still, there are at least two other effects related to photobleaching: the photodegradation (PhD) associated with a lousy alteration of materials induced by light and, also, photobleaching as a consequence of *trans*→*cis* photoisomerization (PhI).²⁷⁻²⁹

Photoinduced transparency can be described as an optical phenomenon in which the absorption decrease when the light irradiance increase. Photoinduced transparency applications generally use SA-related effects instead of PhD and PhI because the process is reversible and tolerable to high light irradiances.

Recently, nanomaterials have attracted attention due to their capability of acting as saturable absorbers with high stability for ultrafast laser pulses. The key requirement for any material to work as a saturable absorber involves a high ratio between the ground (GSA) and excited-state absorption cross-sections. However, solution-grown QDs may present broad size and shape distributions, depending intrinsically on the adopted chemical synthesis method, making it difficult to accurately determine the concentration of nanoparticles in a colloidal solution accurately.³⁰⁻³² Consequently, a wide range of distinct results have been reported on the magnitude of the optical processes occurring in the low-dimensional materials class. Also, the saturable absorption effect in colloidal CdTe QDs has been little explored.^{33, 34} Thus, different optical techniques and a suitable theoretical model were employed to determine the size-dependent photoinduced transparency rate related to ground-state bleaching in aqueous colloidal CdTe QDs capped with the organic stabilizer glutathione.

II – MATERIALS AND METHODS

Glutathione-capped (GSH) CdTe QDs were synthesized through a one-pot aqueous route based on standard colloidal chemistry methods whose details can be found in Refs.^{35, 36}. The ground-state absorption and photoluminescence (PL) spectra were measured on a Shimadzu UV-2550 spectrophotometer and a Shimadzu RF-5301 PC fluorimeter, respectively. Absorption and fluorescence measurements were performed with 10 mm quartz cuvettes containing air-saturated solutions of as-prepared colloidal QDs at room temperature.

We used the fluorescence saturation method to determine the GSA cross-section. For that, we employed as the excitation source 515 nm delivered by an optical parametric amplifier (Orpheus - Light Conversion) pumped by an amplified femtosecond laser system (Pharos - Light Conversion, 1030 nm, 190 fs, 3.0 kHz). The diameter of the laser beam was set 1.6 mm, which was measured through the knife-edge technique. The laser beam reaches the sample (cuvette with 10 mm optical pathway and absorbance of < 0.2 at 515 nm), and the PL is collected at 90° with respect to the incident beam, which is captured through the telescope and an optical fiber coupled to the spectrometer to measure the PL. Because of the high irradiance, a freshly prepared sample was used, and the PL was acquired in the first seconds of excitation to avoid PL photodegradation (fluorescence and absorption spectra were measured after each photoexcitation). The fluorescence lifetime measurements were performed using the same laser system combined with a fast photodetector (700 ps rise time) and a 1GHz oscilloscope.

The SA measurements were carried out by means of an open-aperture Z-scan technique, which uses the same laser system employed in the fluorescence saturation method. The measurements ranged from 480 nm to 620 nm with a repetition rate of 1 kHz. The temporal width of the femtosecond pulses was obtained from the autocorrelator. The samples were placed in 2-mm thick glass cuvettes with a concentration smaller than 2.2×10^{16} QDs/cm³, as will be shown later.

III – RESULTS AND DISCUSSION

The ground-state absorption spectra (solid line-left axis) of the colloidal suspension of GSH-capped CdTe QDs is shown in Fig 1 (a). The position of the absorption band maximum ranges from 520 nm to 565 nm, and is related to the lowest-energy excitonic transition $1S_{3/2}(h) \rightarrow 1S(e)$. The samples were labeled with the number that indicates the wavelength corresponding to the absorption maximum: CdTe-520, CdTe-540, CdTe-550, CdTe-560 and CdTe-565. The redshift (190 meV) from the sample CdTe-520 to CdTe-565 indicates the increase in the QD size. Figure 1 (b) displays the fluorescence spectra excited at the $1S_{3/2}(h) \rightarrow 1S(e)$ transition peak. As noted, the fluorescence spectrum presents a small Stokes-shift and a narrow full-width at half-maximum, characteristics inherent to synthetic procedures based on the colloidal chemistry approach.³⁷

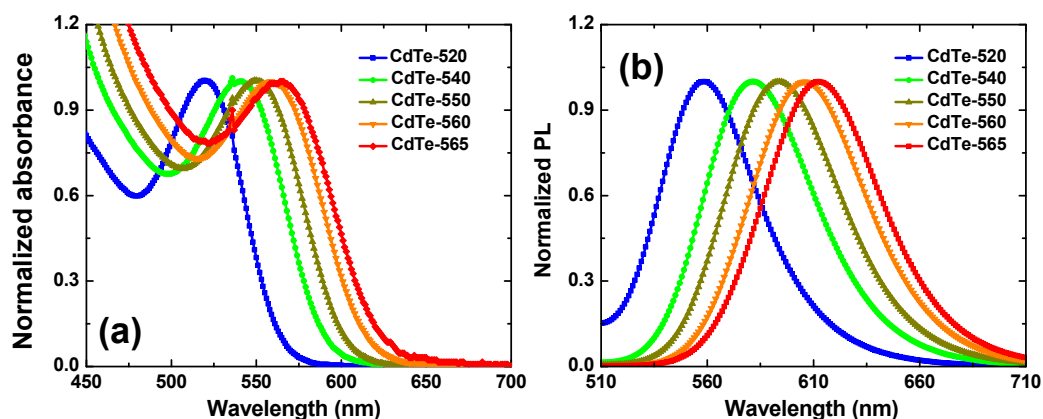


Figure 1 – (a) UV-vis absorption and (b) fluorescence spectra of the synthesized CdTe QD sample.

To determine the average size of our QD samples, we have used a recently developed theoretical methodology that allows converting the measured PL spectrum into realistic estimates for the particle size distribution (PSD) of semiconductor QDs synthesized in a colloidal medium.^{38, 39} Such a spectroscopic model turned out to be particularly accurate for

describing ensembles of nearly spherical colloidal QDs with extremely small sizes (average diameter as small as 1-3 nm), that have not been fully incorporated into the currently available empirical sizing equations.³² The predicted PSDs exhibited an excellent agreement with those obtained from atomic force microscopy (AFM) and transmission electron microscopy (TEM), especially for aqueous CdTe QDs passivated with L-glutathione, which strictly corresponds to the same QD system investigated in the present work.^{38, 39}

Table 1 presents the average particle diameter ($\langle D \rangle$) and relative size dispersion (ξ) resulting from applying the aforementioned methodology to our QD colloidal suspensions. As seen, the average radius of the QD distribution, $\langle R \rangle = \langle D \rangle / 2$, is significantly smaller than the bulk exciton Bohr radius for CdTe ($a_B = 7.5$ nm),⁶ which indicates that the synthesized quantum dots belong to the strong confinement regime ($\bar{R}/a_B \ll 1$).

Table 1: Photophysical parameters for the CdTe QDs studied in this work: absorption peak position, average particle size $\langle D \rangle$, relative size dispersion (ξ), GSA cross section (σ_{he}), the concentration of QDs (C), and electron-hole recombination time (τ_{eh}).

QDs	Absorption peak (eV)	$\langle D \rangle$ (nm)	ξ (%)	σ_{he} (10^{-16} cm ²)	C (QDs/cm ³)	τ_{eh} (ns)
CdTe-520	2.38 (520 nm)	2.33	13.3	3.85 (520 nm)	2.2×10^{16}	39.2
CdTe-540	2.30 (540 nm)	2.62	11.5	4.82 (540 nm)	1.65×10^{16}	45.1
CdTe-550	2.25 (550 nm)	2.75	11.3	4.90 (550 nm)	1.60×10^{16}	46.6
CdTe-560	2.21 (560 nm)	2.88	11.4	5.1 (560 nm)	1.45×10^{16}	48.8
CdTe-565	2.19 (565 nm)	2.95	11.8	5.20 (565 nm)	1.78×10^{16}	52.0

The electronic dynamics concerning the photoinduced transparency for the GSH-capped CdTe-QDs were measured using the femtosecond open aperture Z-scan technique. Figure 2 (a) shows the Z-scan signature for the excitation wavelengths corresponding to the peak of the first excitonic transition. All the Z-scan signatures shown in Fig. 2 were performed using the same average laser power (35 μ W). As can be seen, the normalized transmittance for all curves increases as the sample approaches the focus ($z=0$), which is a characteristic of the saturable absorption (SA) effect configuring the photoinduced transparency. Regarding the SA magnitude, it is observed that it is higher for the smaller QDs.

To aid a deeper understanding of these outcomes and obtain the ground-state bleaching quantitatively, we have considered a three-level energy diagram, as shown in Fig. 2 (b). In such a framework, we have the ground state ($1S_{3/2}(h)$) and two excited states ($1S(e)$ and $nS_{3/2}(e)$), which correspond to the $1S_{3/2}(h) \rightarrow 1S(e)$ and $1S(e) \rightarrow nS_{3/2}(e)$ transitions.

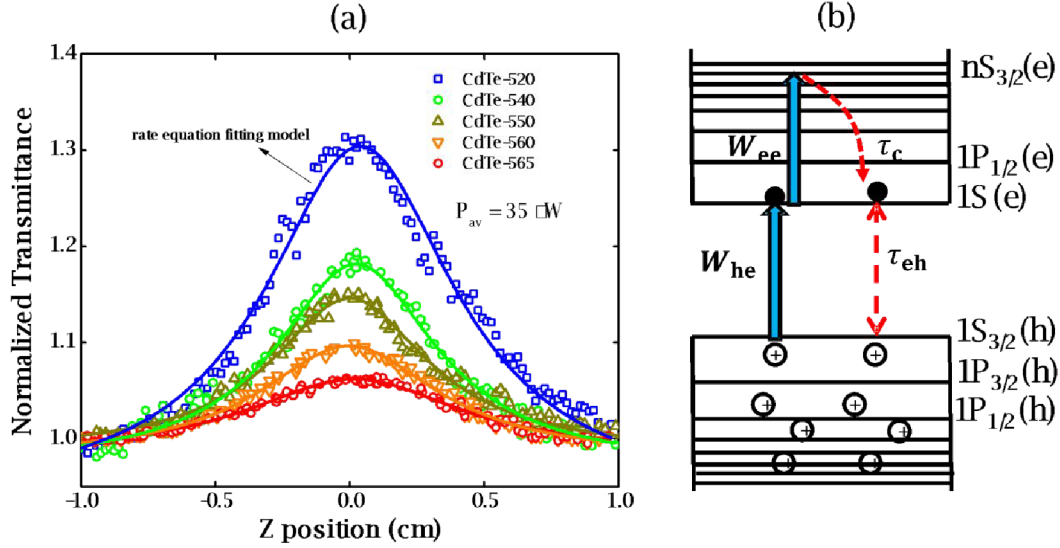


Figure 2 – (a) Femtosecond-laser induced Z-scan signature for the GSH-capped CdTe QDs. Solid lines represent fits to experimental data obtained from the rate equation model. (b) Diagram for the rate equation model within the three-energy level approach used to model the excited state dynamics.

Because the laser pulse duration is much shorter (< 200 fs) than the exciton recombination time ($\tau_{eh} \sim 10^{-9}$ s), electrons excited to the first excited state ($1S(e)$) can be re-excited to the other higher energy excited state ($nS_{3/2}(e)$) with the same laser pulse. It is important to emphasize that the low repetition rate (1 kHz) allows us to avoid thermal effects due to the accumulation of pulses. Thus, the electron population dynamics is ruled by the rate equation model given by:

$$\frac{dn_{1S_{3/2}(h)}(t)}{dt} = -w_{he}(t)n_{1S_{3/2}(h)}(t) + \frac{n_{1S(e)}(t)}{\tau_{eh}}, \quad (1)$$

$$\frac{dn_{1S(e)}(t)}{dt} = +w_{he}(t)n_{1S_{3/2}(h)}(t) - w_{ee}(t)n_{1S(e)}(t) - \frac{n_{1S(e)}(t)}{\tau_{eh}} + \frac{n_{1S(e)}(t)}{\tau_c}, \quad (2)$$

$$\frac{dn_{nS_{3/2}(e)}(t)}{dt} = +w_{ee}(t)n_{1S(e)}(t) - \frac{n_{nS_{3/2}(e)}(t)}{\tau_c}, \quad (3)$$

in which n represent the fraction of the population of each state, with $n_{1S_{3/2}(h)}(t) + n_{1S(e)}(t) + n_{nS(e)}(t) = 1$. The parameters $w_{he} = \sigma_{he}I(t)/h\nu$, and $w_{ee} = \sigma_{ee}I(t)/h\nu$, are the electronic transition rates, $I(t)$ is the laser pulse irradiance, σ_{he} and σ_{ee} are the GSA, bleaching cross-sections, respectively. h and ν are the Planck constant and laser frequency, respectively. The set of coupled differential equations (1-3) is solved numerically, considering the Gaussian time profile of the laser pulse. The temporal dependence of the absorption coefficient during excitation is given by:

$$\alpha(t) = N \{ n_h(t) \sigma_{eh} + n_e(t) \sigma_{ee} \}, \quad (4)$$

in which N is the concentration of QDs (number of particles/cm³). The transmittance is calculated by integrating Beer's law, $dI/dz = -\alpha(t)I(t)$, with respect to the optical pathway z and the temporal width of the laser pulse ($t = -\infty$ to $+\infty$).

In the proposed approach, it is necessary to determine the GSA cross-section (σ_{he}) and, consequently, the concentration of GSH-capped CdTe QDs. However, this is a difficult task to perform accurately because, unlike molecules, colloidal QDs are described by characteristic size distribution functions, thus a great challenge to quantify their concentration. Recently, several works have reported an optical method based on the PL intensity saturation as a function of the irradiance laser.⁴⁰⁻⁴⁴ In this method, when the excitation photon flux ($\langle N \rangle_{photons}$) is very high, i. e., the average number of absorbed photons by exciton ($\langle N \rangle$) is higher than 1, the PL intensity tends to be saturated. Such a condition can be expressed by the following inequality: $\langle N \rangle = \sigma_{he} \langle N \rangle_{photons} > 1$, in which σ_{he} is the GSA cross-section. The referred saturation effect happens because in semiconductor QDs with a high Auger recombination rate as the CdTe QDs, the multi-exciton species have emission intensities much smaller than a single exciton. In this case, the electron-hole pair recombination follows the Poisson statistics given by:⁴¹

$$PL = A \left[1 - e^{-\sigma_{he} \langle N \rangle_{photons}} \right] \quad (5)$$

with

$$\langle N \rangle_{photons} = \frac{P}{f(h\nu)A}, \quad (6)$$

in which PL , P , A and f are, respectively, the PL intensity, the power, spot area, and repetition rate of the excitation laser. It is worth noting that this PL method cannot be applied in QDs with a high Auger recombination rate.⁴¹ Figure 3 (a-e) shows the integrated PL spectra as a function of laser irradiance.

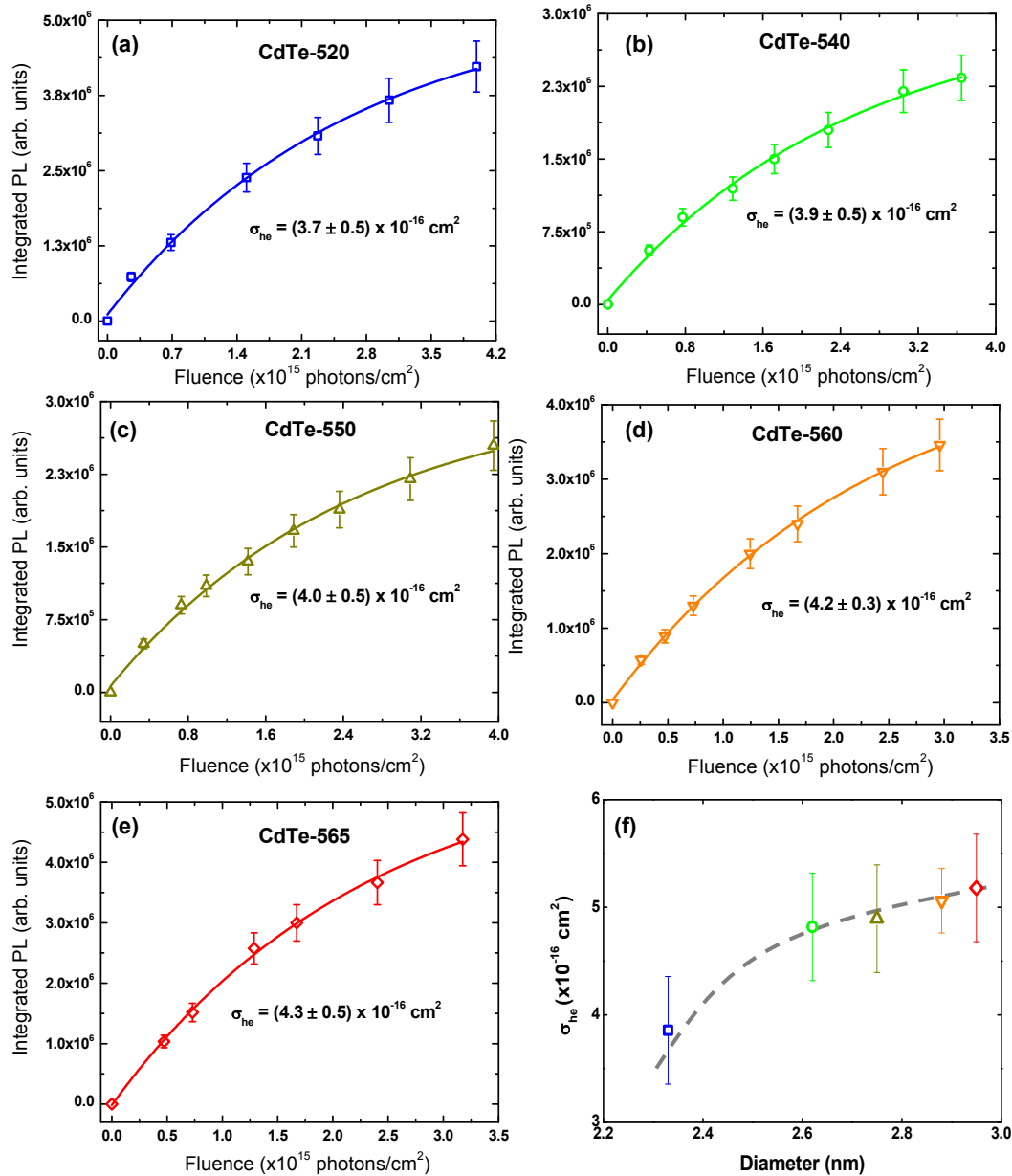


Figure 3 – (a-e) Integrated PL as a function of the laser fluence at 515 nm. (f) GSA cross-section correspondent to the first-excited state transition as a function of the QD diameter. The dashed line is only the eye guide.

As seen, the PL tends to saturate for irradiances higher than 2.0×10^{15} photons/cm², indicating that the multi-exciton species are non-emissive. Through this methodology, we found σ_{he} at

515 nm for all QDs. By using Beer's Law and the GSA spectrum, the σ_{he} values for the other wavelengths were determined. Figure 3 (f) gathers the σ_{he} values related to the first excitonic band peak as a function QDs diameter.

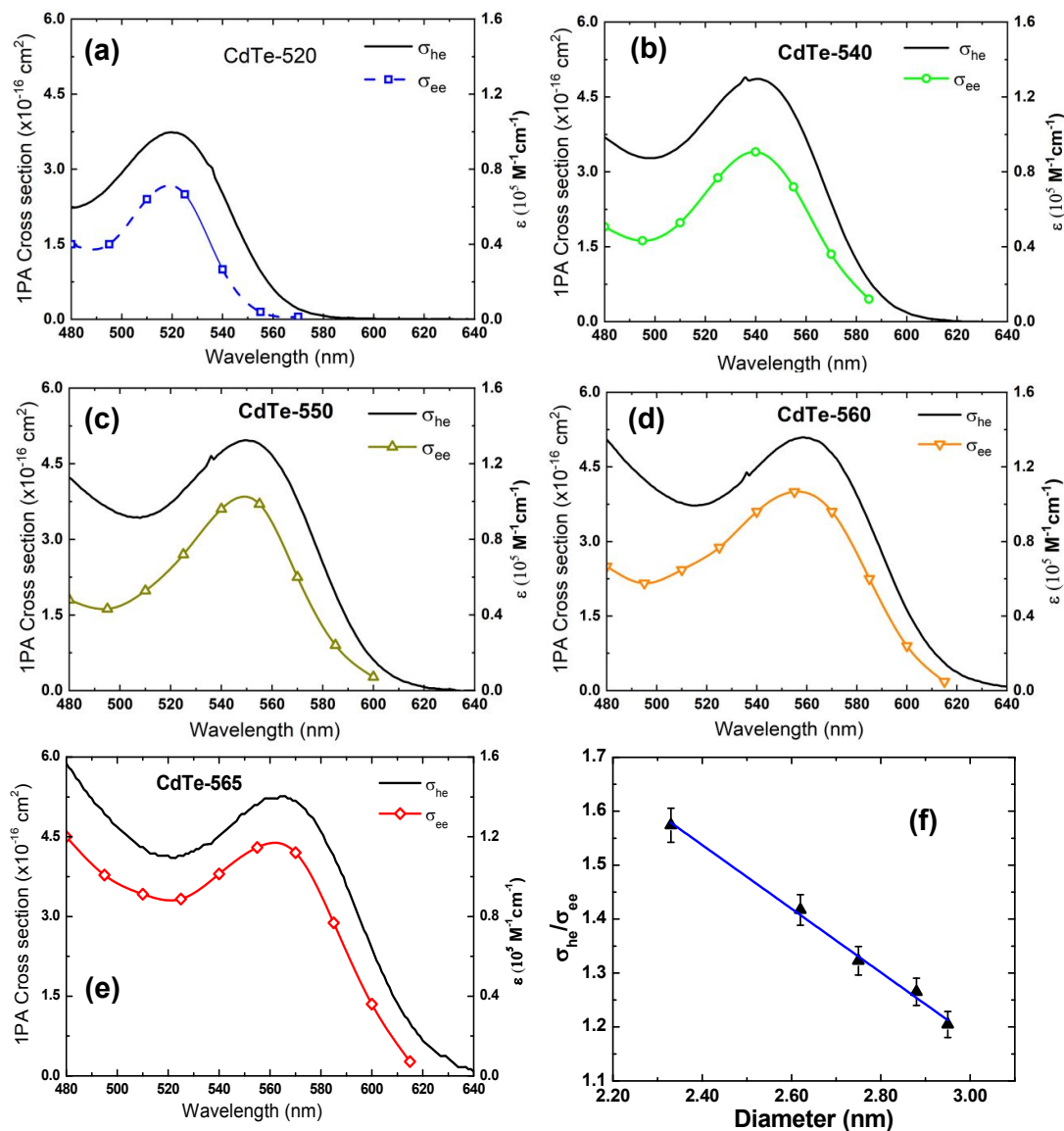


Figure 4 – (a-e) σ_{he} (solid line, ground-state absorption) and σ_{ee} (open dots) spectra for the synthesized colloidal GSH-capped CdTe QDs. (f) $\sigma_{\text{he}}/\sigma_{\text{ee}}$ over the QD diameter. The Z-scan measurements were carried out using low laser power (20-60 μW). The standard deviation of the σ_{ee} cross-section was estimated at 15 %.

The σ_{he} values also are reported in Table 1. We also used this result to calculate the concentration employed in the Z-scan measurements (see Table 1). Furthermore, electron-hole recombination (τ_{he}) and cooling (τ_{c}) times are input parameters in the rate equation

model. The former was obtained through the time-resolved fluorescence technique using femtosecond laser pulses. The τ_{eh} values are reported in Table 1. On the other hand, for the cooling time, we have used $\tau_{\text{c}} = 150$ fs, obtained in Ref. ⁴⁵ by applying the femtosecond transient absorption technique to colloidal CdTe QDs with different sizes. Therefore, all the information necessary to solve Eqs. (1-4) numerically was obtained. Thus, the σ_{ee} parameter can be found unambiguously. Proceeding in this way, in Fig. 2 (a), we show the fits (solid lines) to the Z-scan curves obtained through the rate equation model for the distinct excitation wavelengths. Thus, the σ_{ee} values for the investigated colloidal dispersion of GSH-capped CdTe QDs are displayed in Fig 4 (a-e).

The σ_{ee} values between 480-620 nm for GSH-capped CdTe QDS are on the order of 10^{-16} cm², which is 30-75 % smaller than the corresponding GSA (σ_{he}) value. Therefore, we have $\sigma_{\text{eh}}/\sigma_{\text{ee}}$ between 1.2 and 2.8, which is a moderate SA compared to available cross-section data for organic molecules.^{46, 47} On the other hand, the SA effect here investigated for CdTe QDs is slightly higher than that reported for graphene/polymer composite films and MoS₂, and smaller than black phosphorus nanosheets, also using the femtosecond Z-scan technique.^{48, 49} Table 2 gathers the σ_{eh} and σ_{ee} cross-section to a better comparison among the nanomaterials. It is worth mentioning that among the nanomaterials reported in Table 2, the CdTe QDs have the higher ground-state absorption (σ_{he}) cross-section at the visible region.

Table 2: SA effect for different nanomaterials.

Nanomaterial	$\sigma_{\text{eh}} (\times 10^{-16} \text{ cm}^2)$	$\sigma_{\text{ee}} (\times 10^{-16} \text{ cm}^2)$	$\sigma_{\text{he}}/\sigma_{\text{ee}}$
MoS ₂ ⁴⁹	0.47 ± 0.03 (515 nm)	1.10 ± 0.06 (515 nm)	2.3
Graphene ⁴⁹	0.11 ± 0.03 (515 nm)	0.25 ± 0.03 (515 nm)	2.3
Black phosphorus ⁴⁹	1.25 ± 0.07 (515 nm)	0.30 ± 0.02 (515 nm)	4.1
CdTe <i>this work</i>	4.3 ± 0.4 (490 nm)	1.6 ± 0.2 (490 nm)	2.7

Another interesting aspect to highlight is that σ_{ee} spectra reproduce the same spectral shape as GSA spectra (see Fig. 4), which indicates that ground-state bleaching is the only mechanism associated with the photoinduced transparency. The second one, the photoinduced transparency rate defined here as $\Theta = \sigma_{\text{he}}/\sigma_{\text{ee}}$ has a linear inverse relationship with the QD diameter as depicted in Fig. 4 (f). It is a curious outcome because Θ is directly proportional to the GSA cross-section, which increases over the QD size as shown in Fig. 3 (f). On the other hand, as shown in Ref.⁵⁰, the effective absorption related to the first-excitonic transition for cadmium-based QDs defined by $\alpha_{\text{eff}} = \sigma_{\text{he}}/V$ (which V is the QD volume) is inversely

proportional to the QD diameter. Thus, we show in Fig. 5 that the photoinduced transparency is linearly proportional to the effective absorption coefficient (cross-section values were taken into consideration the peak of the $1S_{3/2}(h) \rightarrow 1S(e)$ excitonic band for each sample).

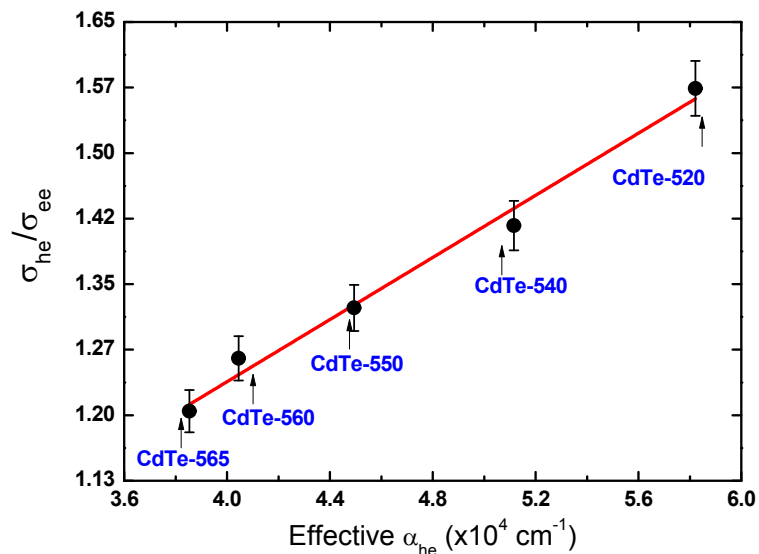


Figure 5 – Transparency photoinduced rate as a function of the effective absorption coefficient for the CdTe QDs considering the peak of the first excitonic band for each sample ($1S_{3/2}(h) \rightarrow 1S(e)$).

IV – FINAL REMARKS

Herein, we combined the femtosecond photoluminescence saturation and Z-scan technique, along with a theoretical approach to size determination, to report the size effect on the photoinduced transparency rate of CdTe-QDs. We have shown that the photoinduced transparency connected to the ground-state bleaching of the CdTe QDs in a strong confinement regime has an inverse linear relationship with the QD diameter. Although counterintuitive, these outcomes are perfectly understood as we calculated the effective absorption coefficient of CdTe QDs. Actually, smaller QDs present higher absorption as we consider their volume, which explains the higher ground-state bleaching observed for them. In a low-concentration ($N < 2 \times 10^{16}$ QDs/cm³) and laser power ($< 35 \mu\text{W}$) regimes, the results have revealed that for the excitation wavelength between 480-620 nm, GSH-capped CdTe QDs exhibit a considerable SA effect, which is slightly higher than graphene, a material widely studied for applications in broadband saturable absorbers for ultrafast lasers. Finally, the presented methodology can be used in excitonic engineering to select the nanomaterial capable of acting as a saturable absorber in ultrafast laser pulse development.

ACKNOWLEDGMENTS

Financial support from FAPEMIG (Fundação de Amparo à Pesquisa do Estado de Minas Gerais, APQ-01469-18), FAPESP (Fundação de Amparo à Pesquisa do Estado de São Paulo, grants 2018/11283-7 and 2015/20032-0), CNPq (Conselho Nacional de Desenvolvimento Científico e Tecnológico, CNPq – Universal Grant 425124/2018-5 and 425180/2018-2), Coordenação de Aperfeiçoamento de Pessoal de Nível Superior (CAPES), Army Research Laboratory (W911NF-21-1-0362) and the Air Force Office of Scientific Research (FA9550-15-1-0521) are acknowledged.

REFERENCES

1. X. P. Zhai, B. Ma, Q. Wang, and H. L. Zhang, *Physical Chemistry Chemical Physics*, 2020, **22**, 22140-22156.
2. J. Z. Li, H. X. Dong, S. F. Zhang, Y. F. Ma, J. Wang, and L. Zhang, *Nanoscale*, 2016, **8**, 16440-16448.
3. Y. H. Qiu, K. Chen, S. J. Ding, F. Nan, Y. J. Lin, J. X. Ma, Z. H. Hao, L. Zhou, and Q. Q. Wang, *Nanoscale*, 2019, **11**, 8538-8545.
4. W. J. Chen, S. Zhang, M. H. Zhou, T. H. Zhao, X. J. Qin, X. F. Liu, M. H. Liu, and P. F. Duan, *Journal of Physical Chemistry Letters*, 2019, **10**, 3290-3295.
5. G. Nagamine, J. O. Rocha, L. G. Bonato, A. F. Nogueira, Z. Zaharieva, A. A. R. Watt, C. H. D. Cruz, and L. A. Padilha, *Journal of Physical Chemistry Letters*, 2018, **9**, 3478-3484.
6. L. A. Padilha, J. Fu, D. J. Hagan, E. W. Van Stryland, C. L. Cesar, L. C. Barbosa, C. H. B. Cruz, D. Buso, and A. Martucci, *Physical Review B*, 2007, **75**.
7. L. A. Padilha *et al.*, *Nano Letters*, 2011, **11**, 1227-1231.
8. L. Protesescu, S. Yakunin, M. I. Bodnarchuk, F. Krieg, R. Caputo, C. H. Hendon, R. X. Yang, A. Walsh, and M. V. Kovalenko, *Nano Letters*, 2015, **15**, 3692-3696.
9. S.-C. Pu, M.-J. Yang, C.-C. Hsu, C.-W. Lai, C.-C. Hsieh, S. H. Lin, Y.-M. Cheng, and P.-T. Chou, *Small*, 2006, **2**, 1308-1313.
10. M. G. Vivas, J. F. Cury, M. A. Schiavon, and C. R. Mendonca, *Journal of Physical Chemistry C*, 2013, **117**, 8530-8535.
11. M. G. Vivas, J. C. L. De Sousa, L. De Boni, M. A. Schiavon, and C. R. Mendonca, *Materials*, 2017, **10**.
12. Y. Q. Xu *et al.*, *Journal of the American Chemical Society*, 2016, **138**, 3761-3768.
13. G. B. dos Reis, R. D. F. Rodriguez, C. I. L. dos Santos, L. A. P. Gontijo, M. A. Schiavon, L. De Boni, C. R. Mendonca, and M. G. Vivas, *Optical Materials*, 2018, **86**, 455-459.
14. V. P. Deviprasad *et al.*, *Journal of Alloys and Compounds*, 2019, **804**, 18-26.
15. J. H. Bang, and P. V. Kamat, *Acs Nano*, 2009, **3**, 1467-1476.
16. C. C. Fu *et al.*, *Proceedings of the National Academy of Sciences of the United States of America*, 2007, **104**, 727-732.
17. X. H. Gao, Y. Y. Cui, R. M. Levenson, L. W. K. Chung, and S. M. Nie, *Nature Biotechnology*, 2004, **22**, 969-976.
18. R. Hanson, L. P. Kouwenhoven, J. R. Petta, S. Tarucha, and L. M. K. Vandersypen, *Reviews of Modern Physics*, 2007, **79**, 1217-1265.

19. P. Lodahl, S. Mahmoodian, and S. Stobbe, *Reviews of Modern Physics*, 2015, **87**, 347-400.
20. S. Yakunin *et al.*, *Nature Communications*, 2015, **6**.
21. T. Yoshie, A. Scherer, J. Hendrickson, G. Khitrova, H. M. Gibbs, G. Rupper, C. Ell, O. B. Shchekin, and D. G. Deppe, *Nature*, 2004, **432**, 200-203.
22. N. X. Ca, N. T. Hien, N. T. Luyen, V. T. K. Lien, L. D. Thanh, P. V. Do, N. Q. Bau, and T. T. Pham, *Journal of Alloys and Compounds*, 2019, **787**, 823-830.
23. S. J. Ding, F. Nan, D. J. Yang, X. L. Liu, Y. L. Wang, L. Zhou, Z. H. Hao, and Q. Q. Wang, *Scientific Reports*, 2015, **5**.
24. W. Z. Wu, S. W. Ren, Q. J. Han, Y. C. Gao, and D. G. Kong, *Physical Chemistry Chemical Physics*, 2018, **20**, 23556-23563.
25. D. Pacifici, H. J. Lezec, and H. A. Atwater, *Nature Photonics* 2007, **1**, 402-406.
26. M. G. Thompson, A. R. Rae, M. Xia, R. V. Penty, and I. H. White, *IEEE J. Sel. Top. Quantum. Electron.*, 2009, **15**, 661-672.
27. M. L. Raicoski, and M. G. Vivas, *Journal of Physical Chemistry B*, 2021, **125**, 9887-9894.
28. L. M. Silva, D. L. Silva, M. V. Boas, Y. Bretonniere, C. Andraud, and M. G. Vivas, *Rsc Advances*, 2020, **10**, 40806-40814.
29. J. N. Henderson, H. W. Ai, R. E. Campbell, and S. J. Remington, *Proceedings of the National Academy of Sciences of the United States of America*, 2007, **104**, 6672-6677.
30. C. D. Donega, and R. Koole, *Journal of Physical Chemistry C*, 2009, **113**, 6511-6520.
31. E. Groeneveld, C. Delerue, G. Allan, Y. M. Niquet, and C. D. Donega, *Journal of Physical Chemistry C*, 2012, **116**, 23160-23167.
32. W. W. Yu, L. H. Qu, W. Z. Guo, and X. G. Peng, *Chemistry of Materials*, 2003, **15**, 2854-2860.
33. J. He, W. Ji, G. H. Ma, S. H. Tang, H. I. Elim, W. X. Sun, Z. H. Zhang, and W. S. Chin, *Journal of Applied Physics*, 2004, **95**, 6381-6386.
34. B. Xu *et al.*, *IEEE Journal of Selected Topics in Quantum Electronics*, 2017, **23**.
35. J. C. L. Sousa, M. G. Vivas, J. L. Ferrari, C. R. Mendonca, and M. A. Schiavon, *Rsc Advances*, 2014, **4**, 36024-36030.
36. Y. Wang, and S. Liu, *Journal of the Chilean Chemical Society*, 2012, **57**, 1109-1112.
37. Y. Pu, F. H. Cai, D. Wang, J. X. Wang, and J. F. Chen, *Industrial & Engineering Chemistry Research*, 2018, **57**, 1790-1802.
38. D. L. Ferreira, R. N. Maronesi, S. O. Ferreira, A. G. Silva, and M. A. Schiavon, *Journal of Physical Chemistry C*, 2019, **123**, 24289-24303.
39. D. L. Ferreira, J. C. L. Sousa, R. N. Maronesi, J. Bettini, M. A. Schiavon, A. Teixeira, and A. G. Silva, *Journal of Chemical Physics*, 2017, **147**.
40. A. Alo, L. W. T. Barros, G. Nagamine, L. B. Vieira, J. H. Chang, B. G. Jeong, W. K. Bae, and L. A. Padilha, *ACS Photonics*, 2020.
41. V. I. Klimov, *Journal of Physical Chemistry B*, 2000, **104**, 6112-6123.
42. V. Krivenkov, P. Samokhvalov, D. Dyagileva, A. Karaulov, and I. Nabiev, *Acs Photonics*, 2020, **7**, 831-836.
43. N. S. Makarov, Q. L. Lin, J. M. Pietryga, I. Robel, and V. I. Klimov, *Acs Nano*, 2016, **10**, 10829-10841.
44. G. Nagamine, H. B. Nunciaroni, H. McDaniel, A. L. Efros, C. H. D. Cruz, and L. A. Padilha, *Nano Letters*, 2018, **18**, 6353-6359.

45. S. Kaniyankandy, S. Rawalekar, S. Verma, D. K. Palit, and H. N. Ghosh, *Physical Chemistry Chemical Physics*, 2010, **12**, 4210-4216.
46. M. G. Vivas, L. De Boni, L. Gaffo, and C. R. Mendonca, *Dyes and Pigments* 2014, **101**, 338-343.
47. M. G. Vivas, E. G. R. Fernandes, M. L. Rodriguez-Mendez, and C. R. Mendonca, *Chem. Phys. Lett.*, 2012, **531**, 173-176.
48. Y. Y. Feng, N. N. Dong, G. Z. Wang, Y. X. Li, S. F. Zhang, K. P. Wang, L. Zhang, W. J. Blau, and J. Wang, *Optics Express*, 2015, **23**, 559-569.
49. S. F. Zhang, Y. X. Li, X. Y. Zhang, N. N. Dong, K. P. Wang, D. M. Hanlon, J. N. Coleman, L. Zhang, and J. Wang, *Nanoscale*, 2016, **8**, 17374-17382.
50. C. A. Leatherdale, W. K. Woo, F. V. Mikulec, and M. G. Bawendi, *Journal of Physical Chemistry B*, 2002, **106**, 7619-7622.